Journal of
Composites Science

MDPI

Article

Flexural Behavior of CFRP Retrofitted Steel Beams: An Experimental Study Including the Components from the Original Champlain Bridge

Mohamadreza Delzendeh [1], Omar Chaallal [1,*] and Brahim Benmokrane [2]

[1] Department of Construction Engineering, École de Technologie Supérieure, University of Quebec, Montreal, QC H3C 1K3, Canada; mohamadreza.delzendeh@polymtl.ca
[2] Department of Civil and Building Engineering, University of Sherbrooke, Sherbrooke, QC J1K 2R1, Canada; brahim.benmokrane@usherbrooke.ca
* Correspondence: omar.chaallal@etsmtl.ca

Abstract

In this study, the flexural behavior of notched steel beams retrofitted with CFRP is investigated. Two series of tests, including W200 × 22 and W14″ wide-flange notched beams rehabilitated with externally bonded (EB) CFRP are evaluated under static loading. The W200 × 22 beams were received directly from a factory, whereas the W14″ wide-flange beams were extracted from the Original Champlain Bridge after roughly 60 years in service. The parameters considered include the CFRP elastic modulus, CFRP configuration, notch depth, anchorage system, and adhesive type. The effect of the CFRP elastic modulus on the rehabilitation technique is examined by using Normal Modulus (NM) and Ultra-High Modulus (UHM) CFRP with approximately the same tensile capacity. Failure modes, load–deflection behavior, strain distributions along the CFRPs, and Crack Mouth Opening Displacement (CMOD) are thoroughly discussed in this study. The results reveal that both UHM and NM CFRP significantly enhance the load-carrying capacity. However, specimens retrofitted with UHM CFRP exhibit a brittle behavior, whereas those strengthened with NM CFRP show a more ductile behavior.

Keywords: experimental study; flexural behavior; notched beams; CFRP rehabilitation technique; steel structures; original bridge elements

1. Introduction

The deterioration of steel bridge structures during their service life is an issue of significant concern. The strength and stiffness, and consequently the capacity of steel components, decrease over time due to fatigue loadings and extreme weather conditions. The conventional method for retrofitting steel structures involves attaching steel plates to the structure using either welding or bolting techniques. However, these conventional techniques are associated with certain disadvantages, including residual stress imposed by welding and susceptibility to corrosion [1–3]. In this context, externally bonded (EB) carbon fiber-reinforced polymers (CFRP) present a promising alternative due to their high strength-to-weight ratio, corrosion resistance and ease of application [4–7]. CFRP is also advantageous for structures where welding could increase the fire risk [8]. CFRPs are classified based on their elastic modulus into Low Modulus (LM), Normal Modulus (NM), High Modulus (HM), and Ultra-High Modulus (UHM). There is no unanimous approach

Check for updates

Academic Editors: Yafei Xu and Xinyu Hui

Received: 23 January 2026
Revised: 19 February 2026
Accepted: 2 March 2026
Published: 5 March 2026

to define the range of the elastic modulus of each category. However, it can be expressed relative to the steel elastic modulus as presented in Table 1 [9].

Table 1. CFRP laminate classification in terms of elastic modulus [9].

Laminate Type	Laminate Modulus	Laminate Modulus Relative to Steel
Low Modulus (LM)	<100 GPa	($E_{CFRP} < 0.5\ E_{steel}$)
Normal Modulus (NM)	100–200 GPa	($0.5\ E_{steel} \leq E_{CFRP} < E_{steel}$)
High Modulus (HM)	200–400 GPa	($E_{steel} \leq E_{CFRP} < 2\ E_{steel}$)
Ultra-High Modulus (UHM)	≥400 GPa	($E_{CFRP} \geq 2\ E_{steel}$)

Several studies have evaluated the application of CFRP in retrofitting steel elements. Yu and Wu [10] investigated the fatigue behavior of cracked steel beams rehabilitated with HM CFRP laminates. Based on experimental results, it was recommended to use nonlinear adhesives (Araldite 420) for the CFRP retrofitting of steel beams, as specimens bonded with linear adhesive (Sikadur-30) were more susceptible to interfacial debonding. The same recommendation was proposed when using NM CFRP as using ductile adhesives is more effective in reducing normal stress at the plate end and improving stress distribution [11].

Zeng et al. [12] analyzed full-scale H-section steel beams strengthened with NM CFRP. The results revealed that local buckling has a notable effect on the load capacity and interfacial shear stress distribution of the steel beams strengthened with CFRP. Selvaraj and Madhavan [13] proposed design limit states for steel beams strengthened with LM CFRP to prevent debonding failure. Furthermore, through experimental studies, intermediate debonding was found to be a dominant failure mode due to the significant modulus difference between steel and LM CFRP. The flexural behavior of steel beams strengthened with NM CFRP sheets using anchorage mechanisms was studied by Kumaraguru and Alagusundaramoorthy [14]. The results showed that CFRP sheets with proper anchorage systems are highly effective in increasing the flexural capacity of steel beams.

The investigation of the flexural behavior of damaged steel beams rehabilitated with prestressed NM CFRP plates revealed that prestressed CFRP plates can significantly improve the load capacity and stiffness of the beams [15]. Moreover, the adhesive layer has a minor impact on the flexural resistance and stiffness of the damaged beams rehabilitated with NM CFRP plates. However, it can contribute to the reliability of the retrofitting system by preventing sudden failures. In another study, it was shown that the unbonded prestressed NM CFRP plates can significantly improve the yielding and ultimate load of the steel-concrete composite beams [16]. It was also found that prestressed NM CFRP can significantly enhance the fatigue life of the steel beams. However, wetting/drying cycles can reduce this improvement [17]. This system can decrease the interfacial stress at the notch location and thereby delay interfacial debonding [18].

Guo, Gao et al. [19] investigated the impact of temperature variations on the performance of NM CFRP retrofitted steel beams. It was found that debonding loads increase as the temperature rises from −20 °C to 60 °C. However, debonding loads decrease at 80 °C due to adhesive softening. Wang, Guo et al. [20] studied the effect of bond slip on the flexural performance of damaged steel beams rehabilitated with NM CFRP and its impact on intermediate debonding using finite element analysis. It was found that interfacial fracture energy is the most critical parameter affecting the flexural retrofitting efficiency compared to maximum bond stress, elastic, and plastic slips. In this regard, increasing the interfacial energy can delay debonding and improve both flexural capacity and ultimate deflection. Comprehensive reviews on the retrofitting of steel structures with CFRP can be found in the literature [8,21–24].

This paper evaluates the flexural behavior of CFRP-rehabilitated notched steel beams, including steel components extracted from the Original Champlain Bridge after more than 60 years in service and fabricated using older steel production practices. The bridge components have been subjected to prolonged periods of loading and unloading, coupled with exposure to harsh weather conditions, thereby adding a distinctive dimension to the research. Furthermore, the effect of CFRP elastic modulus is examined by considering NM and UHM CFRP with roughly the same tensile capacity (2800 MPa × 1.2 mm × 100 mm versus 1500 MPa × 2.2 mm × 100 mm). It should be noted that the elastic modulus and ultimate tensile capacity of CFRPs are inversely related. As a result, a CFRP with a higher elastic modulus requires a greater thickness to achieve the same tensile capacity as a lower modulus CFRP, assuming the width is kept constant. However, increasing the CFRP thickness may intensify stress concentrations and increase the risk of premature debonding. In addition, the effects of CFRP configuration, notch depth, anchorage system, and adhesive type are also investigated in this study. The results are evaluated in terms of failure modes, load–deflection behavior, strain distributions along the CFRPs, and Crack Mouth Opening Displacement (CMOD).

2. Experimental Program

2.1. Material Properties

In this experimental study, two series of steel beams are considered. In the first series, W200 × 22 steel beams of G40.21 44W are used. The height and flange width of the beams are 206 mm and 102 mm, respectively. The thickness of the web and flanges is 6.2 mm and 8 mm, respectively. The total length of the specimens is 1600 mm, and the clear span is 1500 mm. These beams have a yield strength and a minimum tensile strength of 300 MPa and 400–600 MPa, respectively.

In the second series, W14" wide-flange beams of G40.4, extracted from the Original Champlain Bridge in Montreal, are used. The height and width of the beams section are 361 mm and 305 mm, respectively. The thickness of the web and flanges is 10.7 mm and 17.5 mm, respectively. The total length of the specimens is 2250 mm, and the clear span is 2100 mm. These beams have a yield strength and a minimum tensile strength of 230 MPa and 410–500 MPa, respectively.

To rehabilitate the notched steel beams, MAPEI® Carboplate UHM plate and Sika® CarboDur® S512 are applied, representing UHM CFRP and NM CFRP, respectively. The nominal width and thickness of the UHM CFRP plate are 100 mm and 2.2 mm, respectively. The UHM CFRP plate has an elastic modulus of 460 GPa, a tensile strength of 1500 MPa, and an elongation at break of 0.34%. The NM CFRP plate has a nominal width and thickness of 100 mm and 1.2 mm, respectively. The NM CFRP has an elastic modulus of 165 GPa, a tensile strength of 2800 MPa, and an elongation at break of 1.7%. It should be noted that UHM and NM CFRP used in this study have approximately the same tensile capacity (1500 MPa × 2.2 mm × 100 mm versus 2800 MPa × 1.2 mm × 100 mm). To enhance the effectiveness of the rehabilitation technique and prevent CFRP debonding failure, SikaWrap 1400C is used to anchor the CFRP ends. SikaWrap sheets have an elastic modulus of 116 GPa and a tensile strength of 1355 MPa.

To bond the CFRP plates to the steel beams, combined epoxies Fyfe TYFO S (Saturant epoxy) and Fyfe TYFO TC (Tack Coat), which is a ductile adhesive, are used. TYFO S has a tensile strength of 72.4 MPa and a tensile modulus of 3.18 GPa. TYFO TC possesses a tensile strength of 22.7 MPa, a tensile modulus of 1.2 GPa, and a shear strength of 19.3 MPa. Additionally, MapeWrap12 epoxy, which exhibits linear behavior in terms of its stress–strain relationship, is also used to bond CFRP for one specimen. Furthermore, Sikadur 300 with a tensile strength of 55 MPa and a tensile modulus of 1.7 GPa is applied to saturate and bond SikaWrap sheets to the steel beams to anchor the CFRP ends.

Table 2 presents the mechanical properties of the steel beams, CFRPs, and adhesives used to fabricate the specimens. To verify the mechanical properties of the materials provided in datasheets, four steel coupons extracted from each type of beam and five coupons of each adhesive type were tested under tensile tests in accordance with ASTM standards [25,26]. The adhesive and steel coupons are shown in Figure 1, while the stress–strain curves of these coupons are presented in Figure 2.

(**a**) W200×22 beam coupons

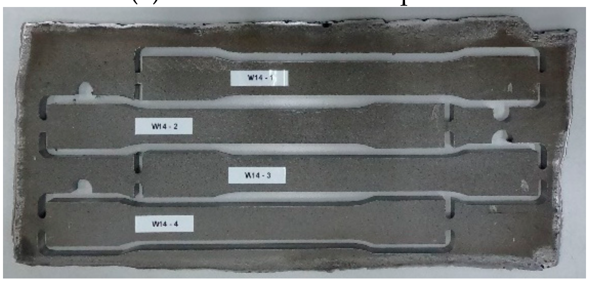

(**b**) W14″ beam coupons

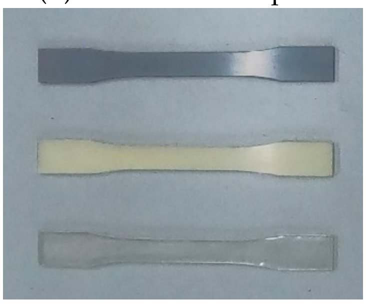

(**c**) Adhesives coupons

Figure 1. Tensile coupon specimens prepared for material characterization.

Table 2. Mechanical properties of materials.

Material	Tensile Strength (MPa)	Tensile Modulus (GPa)	Yield Strength (MPa)
UHM CFRP (MAPEI)	1500	460	NA
NM CFRP (Sika)	2800	165	NA
SikaWrap 1400C	1355	116	NA
Tyfo S (FYFE)	72.4	3.18	NA
Tyfo TC (FYFE)	22.7	1.2	NA
MapeWrap12 (MAPEI)	23.2	-	NA
Sikadur 300	55	1.7	NA
Steel (G40.21 44W)	400–600	~200	300
Steel (G40.4)	410–500	~200	230

NA: Not Applicable

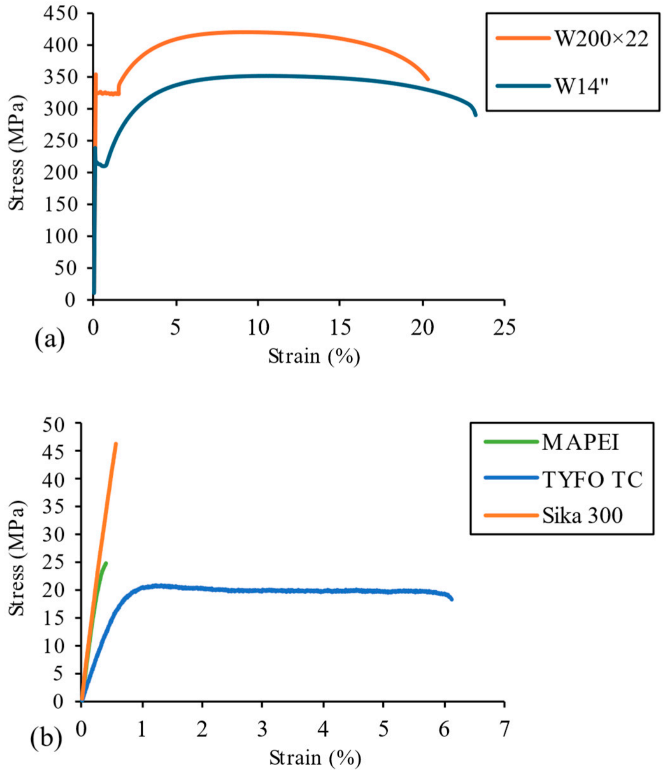

Figure 2. Tensile stress–strain curves of (**a**) the steels and (**b**) adhesives.

2.2. Specimens Preparation

Overall, 21 beams with different notch depths, CFRP elastic moduli, CFRP configurations, and adhesive types were prepared and tested. To avoid local buckling, eight stiffeners were welded on the web at the support and loading points, except for the specimens without anchorage systems. In addition, two different notch depths were applied to the beams. In the first case, the initial notch extends to the beam flange, while in the second case, it extends to the web of the beams.

Surface preparation has been found to be crucial and one of the influential parameters on the bond behavior between CFRP and the steel substrate [27,28]. Therefore, it is important to treat the steel surface to eliminate rust and contaminants, and thereby prevent potential failure at the steel/adhesive interface. Following the guidelines of SSPC SP-10, the bond zones were treated using the sandblasting method. Prior to adhesive application, a thorough cleaning of both the steel surface and CFRP was conducted using acetone to improve mechanical interlocking.

The bonding procedure involves applying TYFO TC to the steel surface using a specifically designed V-notched trowel, ensuring a uniform thickness across all the bond zones. Subsequently, TYFO S was applied to the CFRP plate, which was then bonded to the beam. Once the laminate was in place, it was slightly adjusted to facilitate adhesive spreading and remove any trapped air. For the specimen using MapeWrap12 epoxy, the latter was applied to both the steel and CFRP surfaces. The adhesive thickness is approximately 1 mm, which falls within the 1–2 mm range suggested in the literature [29,30]. After the bonding process, the specimens were cured at room temperature for approximately 14 days before testing [31–33].

The test matrix and specimens labeling are presented in Table 3. As for specimens with the anchorage mechanism, a CFRP sheet (SikaWrap 1400C) was used to anchor the CFRP plate ends, as shown in Figure 3, to increase the efficiency of the retrofitting technique. The schematic view of the CFRP configuration is given in Figure 4. Additionally, the details of each configuration are presented in Table 4.

Table 3. Test matrix and labeling of specimens for flexure test.

Series	No	Specimen	Beam Section	CFRP Type	Epoxy Type	Anchorage	Notch Depth (mm)	CFRP Configuration
Series1	1	W200-REF	W200 × 22	-	-	-	-	-
	2	W200-N6-REF	W200 × 22	-	-	-	6	-
	3	W200-N58-REF	W200 × 22	-	-	-	58	-
	4	W200-N6-UHM-C1	W200 × 22	UHM	TYFO	-	6	Config. 1
	5	W200-N6-NM-C1	W200 × 22	NM	TYFO	-	6	Config. 1
	6	W200-N58-UHM-C2	W200 × 22	UHM	TYFO	-	58	Config. 2
	7	W200-N58-NM-C2	W200 × 22	NM	TYFO	-	58	Config. 2
	8	W200-N6-UHM-C3	W200 × 22	UHM	TYFO	Anchored	6	Config. 3
	9	W200-N6-NM-C3	W200 × 22	NM	TYFO	Anchored	6	Config. 3
	10	W200-N58-UHM-C4	W200 × 22	UHM	TYFO	Anchored	58	Config. 4
	11	W200-N58-NM-C4	W200 × 22	NM	TYFO	Anchored	58	Config. 4
	12	W200-N58-UHM-C5	W200 × 22	UHM	TYFO	Anchored	58	Config. 5
	13	W200-N6-UHM-C3-M	W200 × 22	UHM	MapeWrap12	Anchored	6	Config. 3
Series 2	14	W14-REF	W14″	-	-	-	-	-
	15	W14-N10-REF	W14″	-	-	-	10	-
	16	W14-N160-REF	W14″	-	-	-	160	-
	17	W14-N10-UHM-C1	W14″	UHM	TYFO	Anchored	10	Config. 1
	18	W14-N10-NM-C1	W14″	NM	TYFO	Anchored	10	Config. 1
	19	W14-N160-UHM-C2	W14″	UHM	TYFO	Anchored	160	Config. 2
	20	W14-N160-UHM-C3	W14″	UHM	TYFO	Anchored	160	Config. 3
	21	W14-N160-NM-C3	W14″	NM	TYFO	Anchored	160	Config. 3

Figure 3. Curing of the SikaWrap fabric.

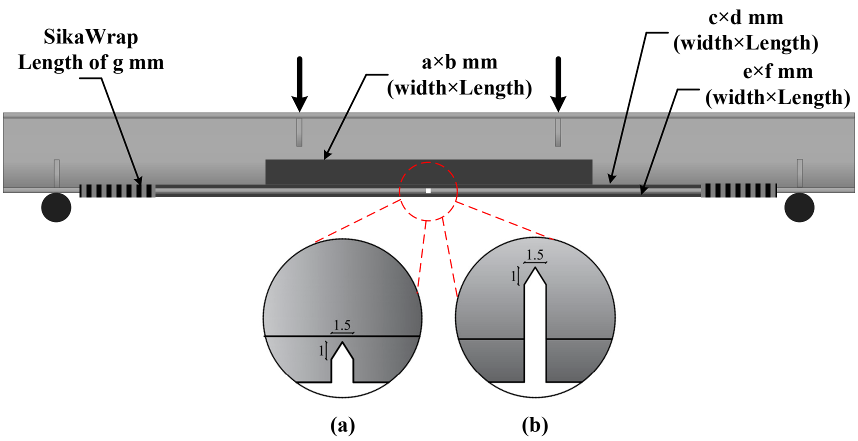

Figure 4. Schematic view of the CFRP configuration and initial notch geometry: (**a**) notch extending to the beam flange; (**b**) notch extending to the beam web.

Table 4. Details of CFRP dimensions used in different configurations.

Beam Section	Configuration	CFRP Dimensions (mm)						
		a	b	c	d	e	f	g
W200 × 22	Config. 1	-	-	-	-	100	800	-
	Config. 2	50	800	-	-	100	800	-
	Config. 3	-	-	-	-	100	1300	200
	Config. 4	80	1000	-	-	100	1300	200
	Config. 5	-	-	47	1300	100	1300	200
W14″ wide flange	Config. 1	-	-	-	-	300	2000	300
	Config. 2	140	1000	-	-	300	2000	300
	Config. 3	-	-	135	2000	300	2000	300

To measure the strain distribution along the CFRP during the flexure test, a series of 20 mm and 30 mm strain gauges was installed on the outer surface of the CFRP plate. Strain gauges were also mounted on the beams to monitor the steel yielding. Displacements at midspan were measured using linear variable differential transducers (LVDTs). In addition, crack gauges were installed to measure the Crack Mouth Opening Displacement (CMOD).

2.3. Test Setup

The beams were tested under four-point flexure using an MTS machine with a capacity of 1200 kN. The test setup is shown in Figure 5. The clear spans are 1500 mm for the W200 × 22 beams and 2100 mm for the W14″ wide-flange beams. The two loading points were placed symmetrically at 500 mm and 700 mm from midspan for the W200 × 22 and W14″ wide-flange beams, respectively. All specimens were loaded at a constant displacement rate of 1 mm/min up to failure.

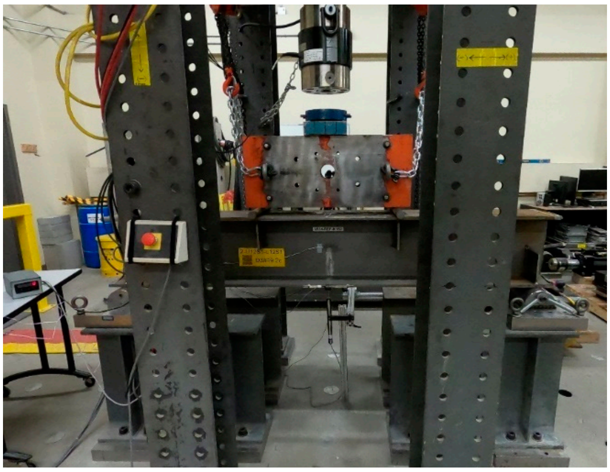

Figure 5. Test setup.

3. Experimental Results

3.1. Failure Modes

The failure modes of the specimens retrofitted with CFRP are presented in Figures 6 and 7. Observations from the tests indicated that cracking sounds were emitted, particularly at higher applied loads for rehabilitated beams. For W200 × 22 beams retrofitted with configurations 1 and 2, the failure mode was the debonding of the CFRP located on the bottom flange for both NM and UHM CFRP, indicating thereby that the CFRPs did not reach their maximum load-carrying capacity. However, the UHM CFRP located on the web underwent rupture while delamination of NM CFRP was observed in configuration 2.

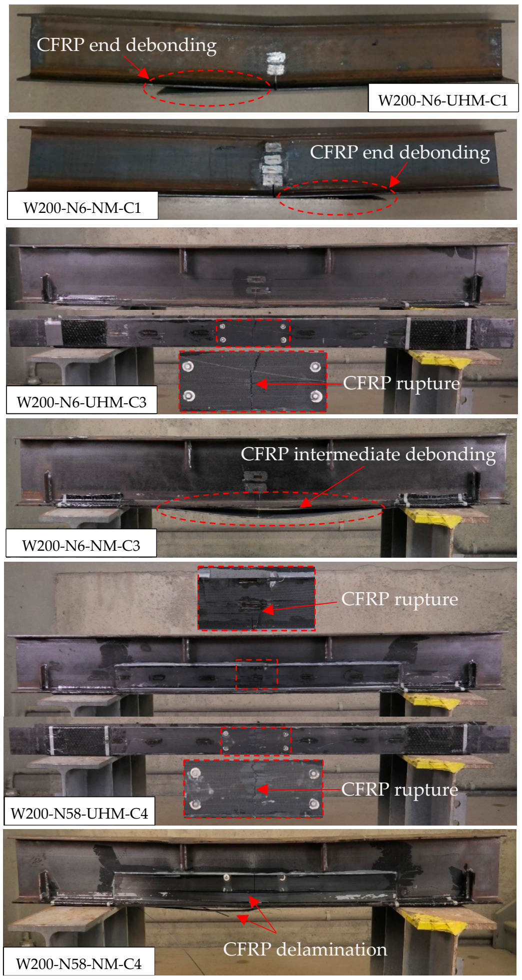

Figure 6. Failure modes of W200 × 22 beams rehabilitated with CFRP.

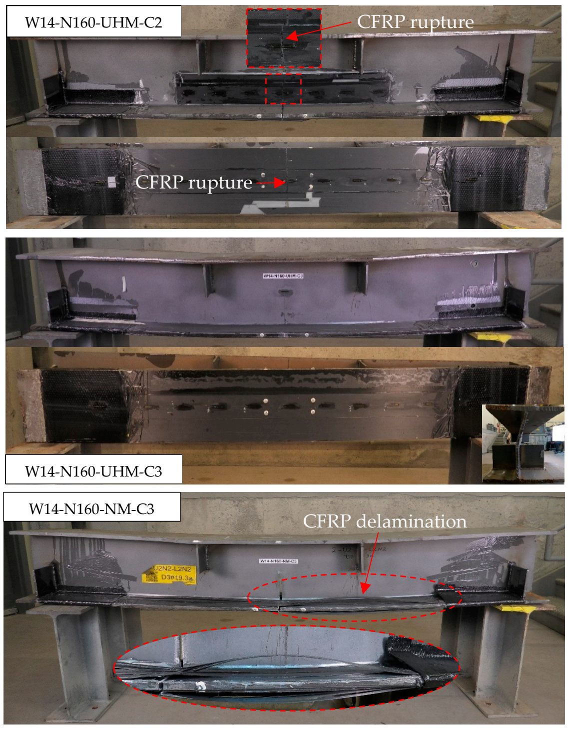

Figure 7. Failure modes of W14″ beams rehabilitated with CFRP.

To enhance the effectiveness of the retrofitting system, several measures were implemented. Firstly, the bond length of the CFRP was increased, allowing for a larger area of contact and improved load transfer between the CFRP and the steel substrate. Additionally, the CFRP ends were anchored using CFRP sheets, preventing thereby premature debonding failure. The failure modes for the enhanced configurations were CFRP rupture for UHM and delamination for NM. However, it is worth mentioning that in specimen W200-N6-NM-C3, intermediate debonding occurred. For configuration 5, it was observed that both UHM CFRPs located on the top and bottom sides of the bottom flange ruptured. As for the specimen with MapeWrap12 epoxy, the failure mode was CFRP rupture. This result indicates that the adhesive type does not affect the failure mode when an effective anchorage system is used. Furthermore, it was observed that only UHM CFRP experienced rupture as a failure mode, while NM CFRP underwent delamination despite reaching its maximum capacity.

Regarding the W14″ beams with an initial notch extending to the beam's flange and with CFRP configuration 1, for both NM and UHM CFRP, the failure mode was identified as flange local buckling on the compression side. This result indicates that the CFRP did not reach its maximum load-carrying capacity, and the steel failed before the CFRP laminate. For W14-N160-UHM-C2, both UHM CFRPs on the web and the bottom flange experienced CFRP rupture. However, in W14-N160-UHM-C3, the steel beams failed due to lateral torsional buckling. It should be noted that the failure in the CFRP rupture case was sudden, whereas specimens with steel failure experienced a more gradual failure process. As for W14-N160-UHM-C3, specimen exhibited CFRP delamination failure between the midspan and the support.

3.2. Load–Deflection Behavior

The load–deflection curves of the specimens are shown in Figure 8. Specimens W200-N6-UHM-C1 and W200-N6-NM-C1, where the initial notch extends to the beam's flange, exhibit load–deflection behaviors similar to REF-6. These results indicate that the CFRP configuration does not contribute to restoring the capacity of the beams. Similarly, in specimens W200-N58-UHM-C2 and W200-N58-NM-C2, the CFRP located on the flange does not effectively restore the flexural capacity. However, a comparison between W200-N6-REF and these specimens reveals that the CFRP applied to the web successfully compensates for the steel loss in the web.

In the case of specimens W200-N6-UHM-C3 and W200-N6-NM-C3, featuring an enhanced configuration, the CFRP effectively restores the capacity of the beams. However, both specimens exhibit brittle behavior, which can be attributed to the lower rupture strain of UHM CFRP. Conversely, the brittle behavior in NM CFRP specimens is due to intermediate debonding. Moving on to specimens W200-N58-UHM-C4 and W200-N58-NM-C4, these demonstrate the successful restoration of the capacity of the beams using the new CFRP configuration. The W200-N58-UHM-C4 specimen exhibits brittle behavior due to the aforementioned reason, whereas the W200-N58-NM-C4 beam displays ductile behavior. Furthermore, it was observed that the UHM CFRP-rehabilitated specimen bonded with linear epoxy exhibited similar behavior compared to the specimen bonded with nonlinear adhesives (specimens W200-N6-UHM-C3 vs. W200-N6-UHM-C3-M).

Regarding the rehabilitation of the steel bridge elements, specimens W14-N10-NM-C1 and W14-N10-UHM-C1, where the initial notch extends to the beam's flange, exhibit load–deflection behaviors similar to W14-REF. This indicates that both types of NM and UHM CFRP effectively contributed to restoring the capacity of the beams. Notably, the beam rehabilitated with UHM CFRP achieved a higher maximum load compared to its counterpart rehabilitated with NM CFRP. Similarly, specimens W14-N160-UHM-C2 and

W14-N160-UHM-C3, where the initial notch extends to the beam's web, successfully restored the flexural capacity. Furthermore, a comparison between these two specimens reveals that the specimens with configuration 2 exhibit brittle behavior and experience a sudden failure after yielding. In contrast, the specimen with configuration 3 features a gradual failure and achieves a higher load-carrying capacity. This discrepancy can be attributed to the location of the CFRP. In configuration 2, the CFRP is bonded to the lower part of the web, whereas in configuration 3, the CFRP is attached to the upper side of the bottom flange. Consequently, bonding CFRP farther from the neutral axis can increase the flexural capacity of the specimens. Moreover, this arrangement can contribute to reducing the interfacial shear stress of the adhesive between the bottom CFRP plate and the steel by shifting the neutral axis to a lower level [34]. It should be noted that CFRP configuration 3 could restore 84% of the load-carrying capacity by compensating for steel loss. The maximum loads achieved by retrofitted W200 × 22 and W14″ wide-flange beams are shown in Figures 9 and 10. As can be seen, the specimens with an anchoring system can successfully restore the capacity of the notched steel beams. Furthermore, the specimens rehabilitated with UHM CFRP generally outperform those rehabilitated with NM in terms of load-carrying capacity, despite the fact that both CFRPs have a similar tensile capacity.

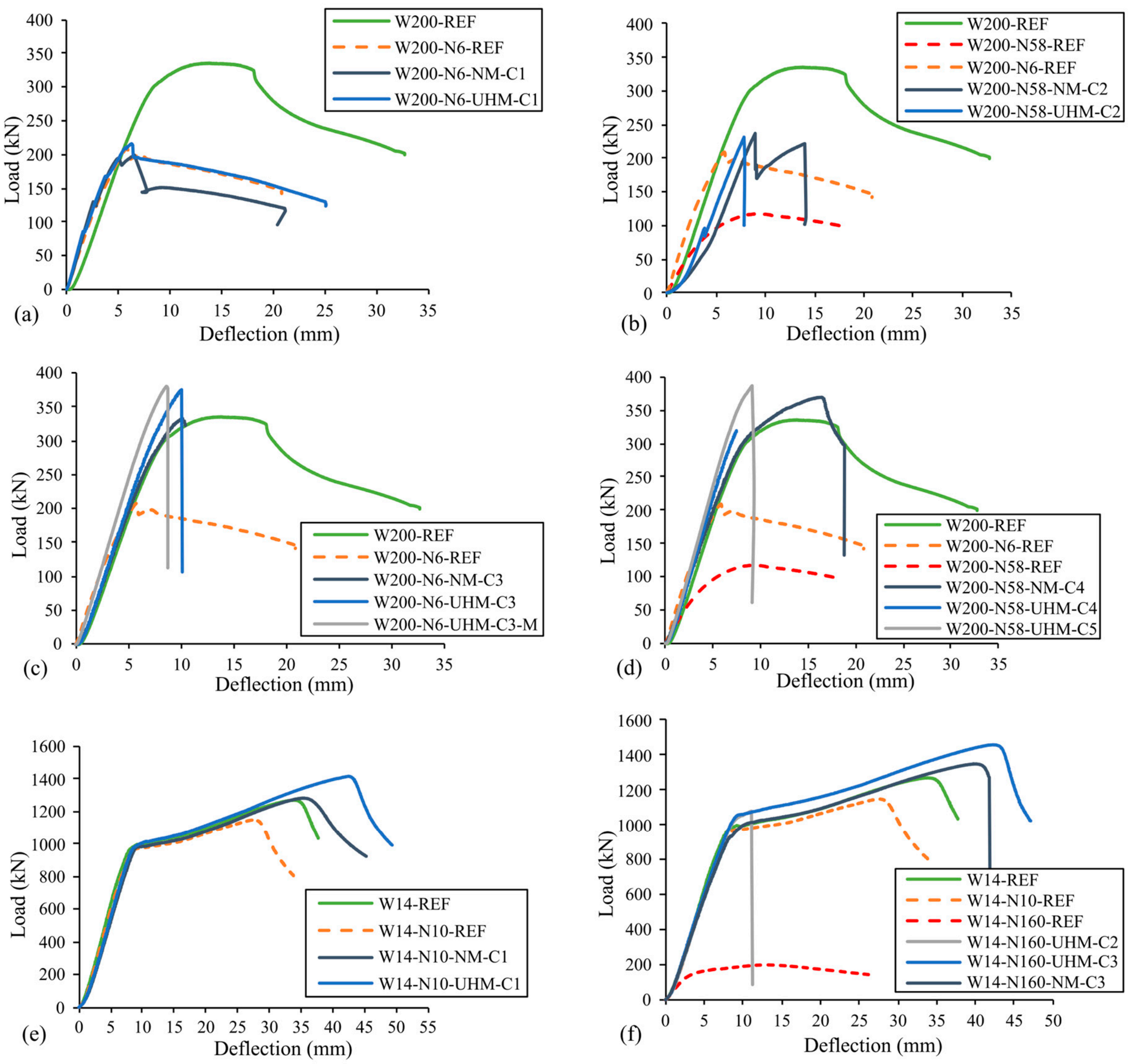

Figure 8. Load–deflection curves: reference vs. rehabilitated beams.

https://doi.org/10.3390/jcs10030138

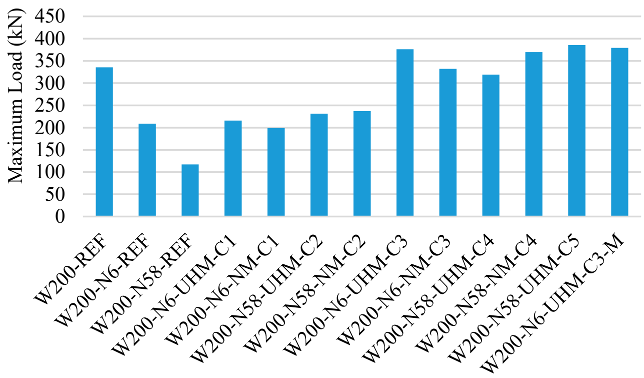

Figure 9. Maximum attained load for reference and rehabilitated W200 × 22 beams.

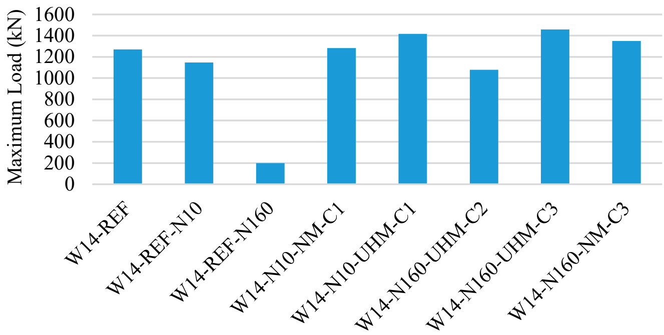

Figure 10. Maximum attained load for reference and rehabilitated W14" wide-flange beams.

3.3. Distributions of CFRP Strains in Beams Rehabilitated with CFRP

Figure 11 presents the strain distributions of the CFRP for the rehabilitated beams with an anchorage system. In the specimens without an anchorage system, debonding was observed at lower load levels, resulting in lower strain experienced by the CFRP compared to the specimens with an anchorage system.

The analysis of the strain distributions along the bonded length reveals that the locations closer to the midspan of the beams exhibited higher strain values compared to those near the supports. This observation clearly indicates that, under monotonic loading, the major part of bond shear resistance takes place in the bonded length section near the midspan, while the shear contribution of intervals closer to the supports is relatively lower. This phenomenon is particularly prominent at load levels approaching the ultimate load capacity of the beams. However, the strain distributions along the bonded length of W14-N10-UHM-C1 specimen shows that locations closer to the loading area exhibited higher strain values compared to those near the supports and the midspan of the beams.

Comparing the strain distributions of the two CFRPs, NM and UHM, it is observed that the maximum strains reached by specimens with NM CFRP were significantly higher than those with UHM CFRP. This is attributed to the higher stiffness of UHM CFRP compared to NM CFRP, which results in lower ductility of UHM CFRP.

Regarding the effect of adhesive type, the results show that using linear and nonlinear adhesives yields similar results when an anchorage system is applied. As can be seen, the strain distribution for both specimens, W200-N6-UHM-C3 and W200-N6-UHM-C3-M, are roughly identical, despite the former being bonded with nonlinear epoxy and the latter with linear epoxy.

https://doi.org/10.3390/jcs10030138

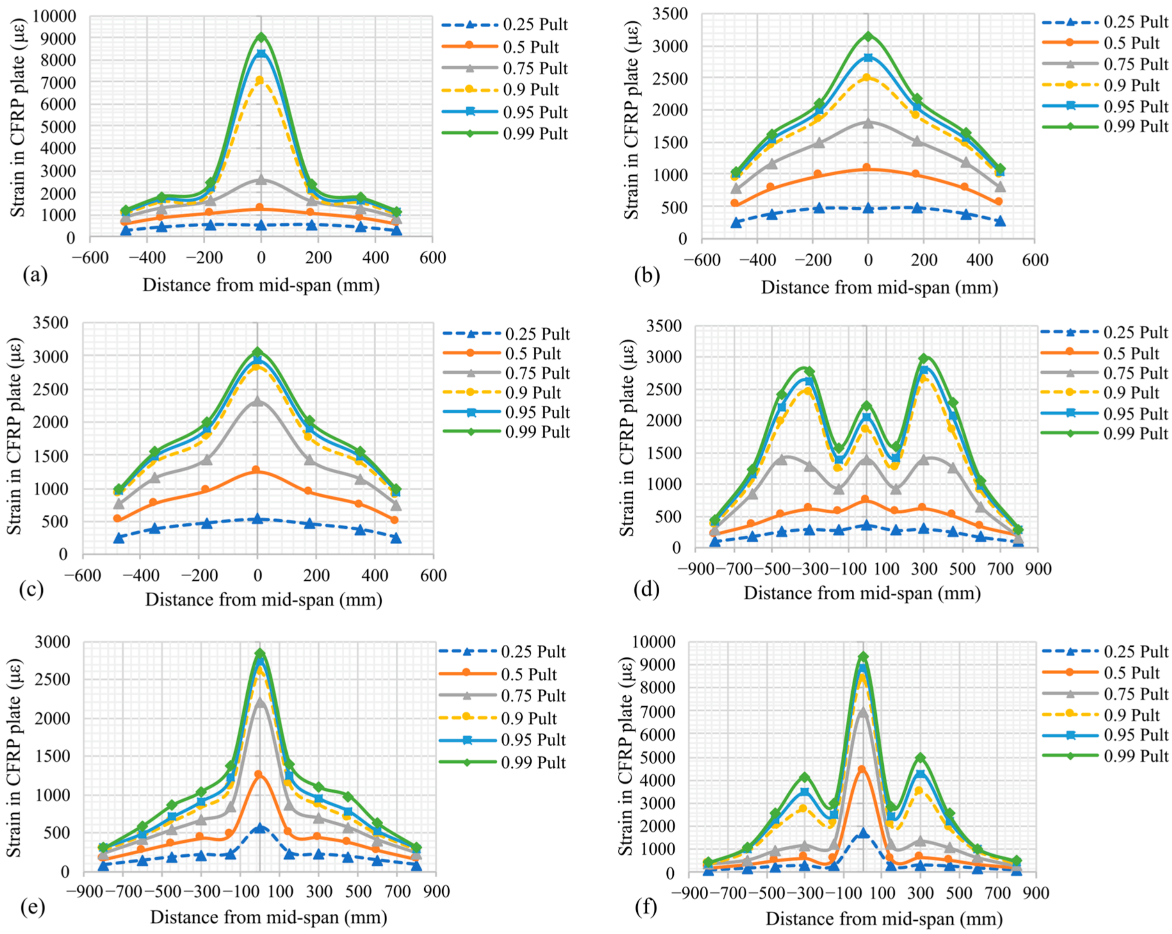

Figure 11. Strain distributions of CFRP located on flange of specimens; (**a**) W200-N6-NM-C3; (**b**) W200-N6-UHM-C3; (**c**) W200-N6-UHM-C3-M; (**d**) W14-N10-UHM-C1; (**e**) W14-N160-UHM-C2; and (**f**) W14-N160-NM-C3.

3.4. Crack Mouth Opening Displacement (CMOD)

Figure 12 shows the load–Crack Mouth Opening Displacement (CMOD) for W200 × 22 rehabilitated beams with an anchorage system. The results indicate that the CFRP rehabilitation technique can effectively control the crack mouth opening. As can be seen, the CMOD increased linearly with load until the failure of the specimens for UHM CFRP-rehabilitated beams. Regarding the effect of adhesive type on the rehabilitation system, both W200-N6-UHM-C3 and W200-N6-UHM-C3-M reached approximately the same peak load and CMOD. This result indicates that, with an effective anchorage system, the type of adhesive does not significantly affect the flexural behavior of the rehabilitated notched beams. The results also show that the specimens rehabilitated with NM CFRP exhibit greater CMOD compared to those retrofitted with UHM CFRP, owing to their more ductile behavior.

Figure 13 presents the CMOD for the W14″ wide-flange rehabilitated beams. A comparison between specimens W14-N10-NM-C1 and W14-N10-UHM-C1 indicates that the specimen rehabilitated with UHM CFRP exhibits a lower CMOD than its NM CFRP counterpart. This result can be attributed to the higher stiffness of the UHM CFRP which contributes to more efficient control of crack opening. Regarding specimens W14-N160-UHM-C2 and W14-N160-UHM-C3, where the initial notch extends to the beam's web, the results show that configuration 3 is more efficient in terms of load-carrying capacity and mitigating crack opening.

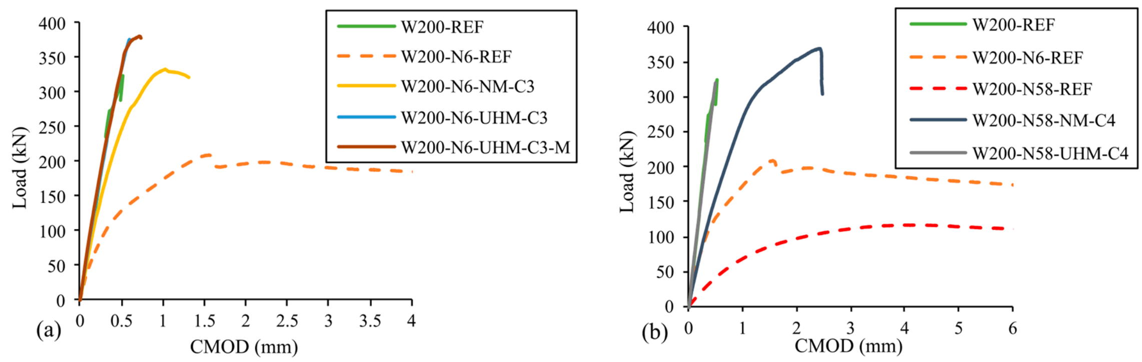

Figure 12. Load–Crack Mouth Opening Displacement: reference vs. W200 × 22 rehabilitated beams.

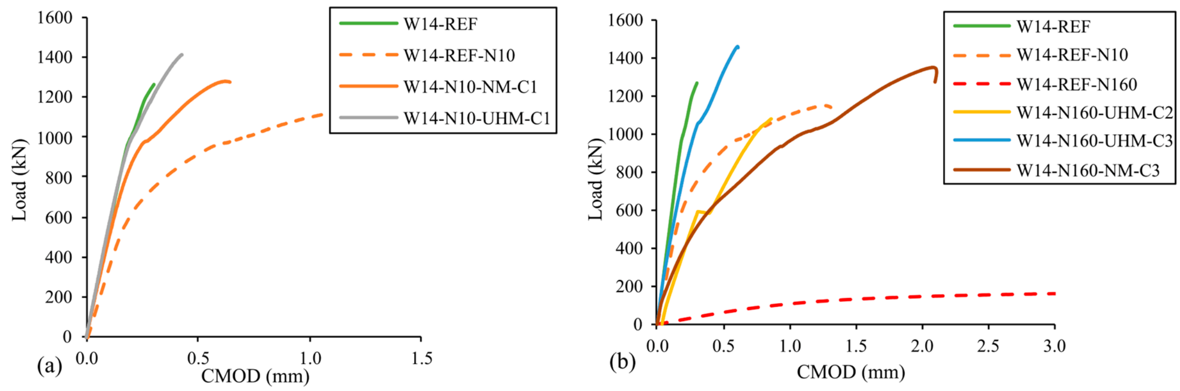

Figure 13. Load–Crack Mouth Opening Displacement: Reference vs. W14" rehabilitated beams.

4. Conclusions

In this study, the flexural behavior of notched steel beams rehabilitated with CFRP was evaluated. In the experimental program various parameters, including the CFRP elastic modulus, anchorage system, adhesive type, and notch depth were considered. Based on the experimental results, the following conclusions can be drawn:

- Specimens bonded with UHM CFRP or NM CFRP without an anchorage system failed by debonding. However, using CFRP sheets as an anchorage system changes the failure mode to CFRP delamination and rupture for NM CFRP and UHM CFRP, respectively. This result indicates that the anchorage system at the CFRP ends successfully prevents premature failure, allowing the CFRP rehabilitation technique to effectively restore the capacity of the notched beams. It is noteworthy that the anchorage system introduced in this study is notably simpler in terms of application compared to the solutions suggested in the existing literature.
- Specimens rehabilitated with UHM CFRP exhibit brittle behavior, while those rehabilitated with NM CFRP feature generally ductile behavior. This difference is attributed to the lower rupture strain of UHM CFRP compared to NM CFRP. Furthermore, a comparison of the failure modes reveals that specimens with UHM CFRP undergo CFRP rupture, whereas those with NM CFRP experience delamination with CFRP breaking longitudinally.
- Both UHM CFRP-rehabilitated specimens bonded with linear and nonlinear adhesives show similar performance in terms of load-carrying capacity, CMOD, strain distribution along the CFRP, and failure mode. This result suggests that the type of adhesive does not significantly alter the flexural behavior of the retrofitted beams when an effective anchorage system is used.

- The findings indicate that the CFRP rehabilitation technique effectively controls crack opening, especially in specimens rehabilitated with UHM CFRP, due to its superior stiffness. Furthermore, UHM CFRP generally outperformed NM CFRP in terms of load-carrying capacity, even though both have approximately the same tensile capacity.
- The results suggest that installing CFRP on both the upper and lower sides of the bottom flange is more efficient when the notch extends into the web. This configuration increases the flexural capacity of the specimens by bonding CFRP farther from the neutral axis. However, in real-life situations, covering the crack on the web of the damaged beam is inevitable, as it guarantees the serviceability of the structure.

Author Contributions: Conceptualization, M.D., O.C. and B.B.; methodology, M.D., O.C. and B.B.; literature review, M.D.; investigation, M.D., O.C. and B.B.; resources, O.C.; writing—original draft preparation, M.D.; writing—review and editing, O.C.; supervision, O.C.; project administration, O.C. and B.B.; and funding acquisition, O.C. All authors have read and agreed to the published version of the manuscript.

Funding: This research was funded by the Natural Sciences and Engineering Research Council of Canada (NSERC), the Fonds de recherche du Québec – Nature et technologies (FRQNT), and Les Ponts Jacques Cartier et Champlain Incorporée (PJCCi).

Data Availability Statement: Some or all data, models, or code that support the findings of this study are available from the corresponding author on reasonable request.

Acknowledgments: The authors gratefully acknowledge the financial support of the Natural Sciences and Engineering Research Council of Canada (NSERC) and the Fonds de Recherche du Québec—Nature et Technologies (FRQNT). The authors also wish to express their sincere appreciation to the Jacques Cartier and Champlain Bridges Incorporated (PJCCI) for their generous financial and material support, which made this study possible. In addition, the authors would like to thank Sika Canada and MAPEI Canada for their valuable contributions of materials.

Conflicts of Interest: The authors declare no conflicts of interest.

References

1. Schnerch, D.; Dawood, M.; Rizkalla, S.; Sumner, E. Proposed design guidelines for strengthening of steel bridges with FRP materials. *Constr. Build. Mater.* **2007**, *21*, 1001–1010. [CrossRef]
2. Fisher, J.W. Evolution of fatigue-resistant steel bridges. *Transp. Res. Rec.* **1997**, *1594*, 5–17. [CrossRef]
3. Dexter, R.J.; Ocel, J.M. *Manual for Repair and Retrofit of Fatigue Cracks in Steel Bridges*; Federal Highway Administration: Washington, DC, USA, 2013.
4. Oudah, F.; El-Hacha, R. Research progress on the fatigue performance of RC beams strengthened in flexure using Fiber Reinforced Polymers. *Compos. Part B Eng.* **2013**, *47*, 82–95. [CrossRef]
5. Chataigner, S.; Benzarti, K.; Foret, G.; Caron, J.; Gemignani, G.; Brugiolo, M.; Calderon, I.; Piñero, I.; Birtel, V.; Lehmann, F. Design and testing of an adhesively bonded CFRP strengthening system for steel structures. *Eng. Struct.* **2018**, *177*, 556–565. [CrossRef]
6. Hu, B.; Li, Y.; Jiang, Y.-T.; Tang, H.-Z. Bond behavior of hybrid FRP-to-steel joints. *Compos. Struct.* **2020**, *237*, 111936. [CrossRef]
7. Wang, H.-T.; Liu, S.-S.; Liu, Q.-L.; Pang, Y.-Y.; Shi, J.-W. Influences of the joint and epoxy adhesive type on the CFRP-steel interfacial behavior. *J. Build. Eng.* **2021**, *43*, 103167. [CrossRef]
8. Teng, J.G.; Yu, T.; Fernando, D. Strengthening of steel structures with fiber-reinforced polymer composites. *J. Constr. Steel Res.* **2012**, *78*, 131–143. [CrossRef]
9. Ghafoori, E.; Motavalli, M. Normal, high and ultra-high modulus carbon fiber-reinforced polymer laminates for bonded and un-bonded strengthening of steel beams. *Mater. Des.* **2015**, *67*, 232–243. [CrossRef]
10. Yu, Q.-Q.; Wu, Y.-F. Fatigue retrofitting of cracked steel beams with CFRP laminates. *Compos. Struct.* **2018**, *192*, 232–244. [CrossRef]
11. Wang, Z.; Xian, G.; Yue, Q. Finite element modeling of debonding failure in CFRP-strengthened steel beam using a ductile adhesive. *Compos. Struct.* **2023**, *311*, 116818. [CrossRef]
12. Zeng, J.-J.; Gao, W.-Y.; Liu, F. Interfacial behavior and debonding failures of full-scale CFRP-strengthened H-section steel beams. *Compos. Struct.* **2018**, *201*, 540–552. [CrossRef]

13. Selvaraj, S.; Madhavan, M. Design of Steel Beams Strengthened with Low-Modulus CFRP Laminates. *J. Compos. Constr.* **2020**, *24*, 04019052. [CrossRef]
14. Kumaraguru, S.; Alagusundaramoorthy, P. Flexural strengthening of steel beams using pultruded CFRP composite sheets with anchorage mechanisms. *Structures* **2021**, *33*, 1414–1427. [CrossRef]
15. Wang, H.-T.; Bian, Z.-N.; Chen, M.-S.; Hu, L.; Wu, Q. Flexural strengthening of damaged steel beams with prestressed CFRP plates using a novel prestressing system. *Eng. Struct.* **2023**, *284*, 115953. [CrossRef]
16. Qiang, X.; Chen, L.; Jiang, X. Experimental and theoretical study on flexural behavior of steel–concrete composite beams strengthened by CFRP plates with unbonded retrofit systems. *Compos. Struct.* **2023**, *309*, 116763. [CrossRef]
17. Deng, J.; Li, J.; Zhu, M. Fatigue behavior of notched steel beams strengthened by a prestressed CFRP plate subjected to wetting/drying cycles. *Compos. Part B Eng.* **2022**, *230*, 109491. [CrossRef]
18. Li, J.; Zhu, M.; Deng, J. Flexural behaviour of notched steel beams strengthened with a prestressed CFRP plate subjected to fatigue damage and wetting/drying cycles. *Eng. Struct.* **2022**, *250*, 113430. [CrossRef]
19. Guo, D.; Gao, W.-Y.; Liu, Y.-L.; Dai, J.-G. Intermediate crack-induced debonding in CFRP-retrofitted notched steel beams at different service temperatures: Experimental test and finite element modeling. *Compos. Struct.* **2023**, *304*, 116388. [CrossRef]
20. Wang, H.-T.; Guo, C.-C.; Liu, Q.-L.; Wu, Q. Influences of the bond-slip on the flexural performance of CFRP plate-strengthened damaged steel beams with intermediate debonding: A numerical study. *Structures* **2023**, *58*, 105661. [CrossRef]
21. Delzendeh Moghadam, M.; Fathi, A.; Chaallal, O. Retrofitting of Steel Structures with CFRP: Literature Review and Research Needs. *Appl. Sci.* **2024**, *14*, 5958. [CrossRef]
22. Borrie, D.; Al-Saadi, S.; Zhao, X.-L.; Raman, R.K.S.; Bai, Y. Bonded CFRP/Steel Systems, Remedies of Bond Degradation and Behaviour of CFRP Repaired Steel: An Overview. *Polymers* **2021**, *13*, 1533. [CrossRef] [PubMed]
23. Zhao, X.-L.; Zhang, L. State-of-the-art review on FRP strengthened steel structures. *Eng. Struct.* **2007**, *29*, 1808–1823. [CrossRef]
24. Gholami, M.; Sam, A.R.M.; Yatim, J.M.; Tahir, M.M. A review on steel/CFRP strengthening systems focusing environmental performance. *Constr. Build. Mater.* **2013**, *47*, 301–310. [CrossRef]
25. *ASTM-A370*; Standard Test Methods and Definitions for Mechanical Testing of Steel Products. ASTM International Designation: West Conshohocken, PA, USA, 2020.
26. *ASTM-D638*; Standard Test Method for Tensile Properties of Plastics. ASTM International Designation: West Conshohocken, PA, USA, 2014.
27. Fernando, D.; Teng, J.G.; Yu, T.; Zhao, X.L. Preparation and characterization of steel surfaces for adhesive bonding. *J. Compos. Constr.* **2013**, *17*, 04013012. [CrossRef]
28. Russian, O.; Khan, S.; Belarbi, A.; Dawood, M. Effect of surface preparation technique on bond behavior of CFRP-steel double-lap joints: Experimental and numerical studies. *Compos. Struct.* **2021**, *255*, 113048. [CrossRef]
29. *The Structural Use of Adhesives*; The Institution of Structural Engineers (ISE): London, UK, 1999.
30. Xia, S.; Teng, J. Behaviour of FRP-to-steel bonded joints. In Proceedings of the International Symposium on Bond Behaviour of FRP in Structures, BBFS 2005, Hong Kong, China, 7–9 December 2005; International Institute for FRP in Construction (IIFC): Kingston, ON, Canada, 2005.
31. Yu, T.; Fernando, D.; Teng, J.G.; Zhao, X.L. Experimental study on CFRP-to-steel bonded interfaces. *Compos. Part B Eng.* **2012**, *43*, 2279–2289. [CrossRef]
32. Wang, H.-T.; Wu, G.; Dai, Y.-T.; He, X.-Y. Determination of the bond–slip behavior of CFRP-to-steel bonded interfaces using digital image correlation. *J. Reinf. Plast. Compos.* **2016**, *35*, 1353–1367. [CrossRef]
33. Yang, Y.; Zhao, J.; Zhang, S.; Chastre, C.; Biscaia, H. Effect of mechanical anchorage on the bond performance of double overlapped CFRP-to-steel joints. *Compos. Struct.* **2021**, *267*, 113902. [CrossRef]
34. Al-Saidy, A.H. *Structural Behavior of Composite Steel Beams Strengthened/Repaired with Carbon Fiber Reinforced Polymer Plates*; Iowa State University: Ames, IA, USA, 2001.